Design and Characterization of the Seashell Effect Pretouch Sensor Integrated Into Robot Grippers

Liang-Ting Jiang
Department of Mechanical Engineering
University of Washington
Seattle, USA
email: jianglt@uw.edu

Joshua R. Smith
Department of Computer Science and Engineering
Department of Electrical Engineering
University of Washington
Seattle, USA
email: jrs@cs.uw.edu

***Abstract*—The paper presents a short range proximity pretouch sensor device based on the seashell effect inspired by the phenomenon of "hearing the sea" when a seashell is held to the ear. The acoustic theory, design consideration, and the quantitative characterizations of the sensor under different ambient sound conditions are studied. The sensor has a number of practical benefits compared to conventional sonar-based time of flight sensors: (1) easy sensor integration — the sound stimulus source and the detector do not need to be co-located; (2) short-time measurements are not required; (3) no multi-path effects. The sensors are designed and integrated into a robot's gripper, which provides a new source of information for robotic manipulation that complements long range depth sensors and contact-based tactile sensors. Continuous object contour tracking using differential measurements with pairs of the new sensors (one in each robot's fingertip) is demonstrated on objects with different material properties.**

Keywords–pretouch; sensor; acoustic; proximity; non-contact

I. INTRODUCTION

"Pretouch" sensors are non-contact sensors with properties intermediate between long range non-contact sensors (RGB cameras, depth cameras, and laser rangefinders) and contact-based tactile sensors. Previous pretouch sensors based on electric field [1][2][3] and optics [4] have been used in several robot grasping applications, such as robot hand preshaping, gripper servoing, co-manipulation, and, mid-range object imaging. One issue of these sensors is their restricted compatibility for different material properties. Electric field pretouch only works well on materials with high conductivity or dielectric constant, and optical methods (including optical pretouch as well as RGB cameras and depth sensors) are not suited to highly reflective, transparent, or absorbing (black) materials.

The "seashell effect pretouch" sensor [5] we previously proposed relies on mechanical (acoustic) properties rather than electrical or optical properties, and, therefore, is compatible with a set of materials that is orthogonal to those can be sensed by electrical / RF or optical techniques. The effectiveness of seashell effect pretouch was demonstrated with two simple robot grasping applications: (1) pretouch-assisted grasp planning, in which the pretouch sensor is used to exhaustively augment the point cloud of the object provided by a depth sensor operating in sub-optimal conditions, such as with transparent materials or occluded objects; (2) reactive grasping: the detection of extremely compliant objects which can not be sensed by traditional tactile sensors. Recently, we also proposed a unified probabilistic framework to enable automatic exploration with the pretouch sensor to reduce object shape uncertainty before robotic grasping [6].

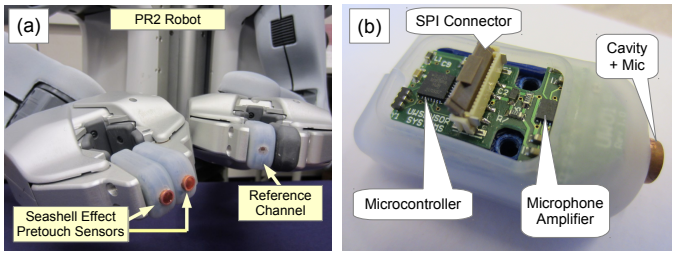

Fig. 1. (a) The seashell effect pretouch sensors installed on the Willow Garage PR2 robot grippers. (b) The sensor system consists of a PCB, a microcontroller, electronic components, a microphone, and an acoustic cavity integrated into the PR2 robot's fingertip.

In this paper, we further discuss in more detail the acoustic theory, design consideration, and the quantitative characterizations of the sensor. We also characterizes the effect of ambient noise power and spectral contents on the sensor performance, and propose an adaptive stimulus generation by deliberately generating white noise, band limited to match the sensor's frequency response. It detects current ambient sound conditions and provides additional band-limited white noise to maintain consistent SNR ratio, and thus guarantee minimum sensor performance, even at low ambient sound levels. We also introduce an embedded sensor system integrated into the PR2 robot's gripper, which eliminates the external power and data cables necessary in prior implementations. This improved implementation has also made it practical to integrate multiple seashell effect sensors in a single robot (one in each finger).

The paper is organized as follows: in Section II, we first review the related work. The acoustic theory is discussed in Section III. The sensor design and considerations are discussed in detail in Section IV, and then the proposed sensor systems is characterized in Section V. In Section VI, we show an example application of the proposed sensor in robotics. Finally, in Section VII, we conclude and discuss the future work.

II. RELATED WORK

The idea of acoustic resonant shift is widely used in highly sensitive mass sensors for chemical and biological environment [7]. A typical acoustic mass sensor uses the fact that the

 ISBN: 978-1-61208-297-4

resonant frequency of an acoustic-wave resonator changes in response to the mass load applied on the resonator's surface. For example, Zhang et al. [8][9] devised a micromachined film bulk acoustic resonator mass sensor built on a micromachined silicon-nitride diaphragm with a piezoelectric thin film and Al electrodes that can operate in vapor and liquid. Its resonant frequency drops linearly with added mass on the surface. The shift of the acoustic resonant frequency is measured from the longitudinal standing wave existing between two faces of the electrodes sandwiching a piezoelectric film, and the mass load and be inferred from the frequency shift.

In the design of our seashell effect pretouch sensor, we design an acoustic system (a closed-open ended cylindrical pipe in our case), in which its resonant frequency is shifted by the reactive radiation impedance (small vibrating air mass) change at the open termination of the pipe caused by the obstacle.

III. Acoustic Theory

The seashell effect is the phenomenon of "hearing the sea" that is observed when a seashell is held to the ear. The sound is the ambient noise amplified (attenuated) with the seashell cavity's acoustic frequency response. Inspired by the fact that the sound of the sea changes as the distance from the seashell to the head varies, a pretouch sensor is essentially an acoustic cavity (an closed-open pipe in our case) attached to a microphone that detects the change in ambient sound spectrum that occurs when the pipe approaches an object. When an object approaches the pipe opening, the sound field between the surface of the object and the pipe opening causes a change in the effective (acoustic) length of the pipe. Perhaps counterintuitively, the effective length of the pipe increases as the sensed object approaches; thus the resonant frequency of the pipe decreases as an object approaches. The similar effects were also studied for the woodwind musical intruments which have keys (buttons) hanging above the tone holes [10]. The key acoustic theory is summarized in this section.

A. End Correction of Cylindrical Pipes

The shift of the resonant frequency caused by the object can be best explained by using the terminologies of acoustic impedance and end correction. The acoustic impedance is defined as: $Z = \frac{P}{U}$, where P and U are the amplitude of the sound pressure and volume velocity, respectively. For an ideal closed-open pipe, the closed end is a rigid termination with infinity acoustic impedance ($Z_c = \infty$). At the open end, the sound wave is small compared to the atmospheric pressure, so the open end acts as a release termination at which the pressure vanishes (p = 0) with zero acoustic impedance ($Z_o = 0$), which gives total reflection in anti-phase. However, the open end is in fact terminated by a radiation impedance. The effect of radiation can be approximated by considering the wave in the pipe accelerating the final layer of the air back and forth as a small mass. The radiation impedance (Z_r) seen by this final layer has a general form of:

$$Z_r = \frac{Z_0}{S}(R + jX) \tag{1}$$

where Z_0 is the characteristic impedance (Z_0 = 415 Ns/m^3 for air at 20 °C); $S = \pi a^2$ is the area of the pipe (m^2), where a is the pipe radius; R and X are functions of the wave number k, the pipe radius a, and most importantly, the geometric configuration in the environment around the opening. R and X represent the similar ratios of the real part of the impedance (acoustic resistance) and the imaginary part of the impedance (acoustic reactance) to the characterisric impedance, respectively. The imaginary part corresponds to the impedance of a mass of a volume of the medium of the size $S\Delta L$, and shifts the position where reflection in antiphase occurs to a virtual plane outside the tube by ΔL, which is usually called *end correction*. The end correction ΔL= $0.8488a$ for a cylinder pipe with infinite flange can be solve analytically using Rayleigh integral for the Helmholtz equation [11], and serves as the upper bound for cylindrical pipes, while ΔL= $0.6133a$ for cylindrical unflange pipe [12] was solved under plane wave assumption (for frequency lower than the first cut-off frequency of the pipe), which serves as the lower bound. End correction for other complicated geometric configurations are usually found by numerical and experimental methods [13].

In our application, we are most interested in knowing the effects of obstacles presenting near the opening, specifically, the distance of the object to the opening. The presented object further restricts the space for sound wave propagation and causes more end correction in addition to ΔL. Dalmont et. al. [14] presented an emperical formula of this additioanl end correction term ΔL_{obj} for this situation:

$$\Delta L_{obj} = \frac{a}{3.5(h/a)^{0.8}(h/a + 3w/a)^{-0.4} + 30(h/d)^{2.6}} \tag{2}$$

where a is the radius of the pipe; h is the distance between the obstable and the pipe opening; w is the thickness of the pipe wall; d is the width of the object. Considering this additional end correction, the effective length of the pipe becomes:

$$L_{eff} = L + \Delta L + \Delta L_{obj} \tag{3}$$

B. Resonance Frequency

The fundamental resonance frequency of the standing wave in a closed-open pipe f_0 can be found by

$$f_0 = \frac{c}{4L_{eff}} \tag{4}$$

where c is the speed of sound. The effective pipe lenght is altered when an object is presented near the opening. Therefore, by measuring the resonance frequency of the pipe, we can inversely infer effective length of the pipe, and then further infer the distance of the object h from experimental data.

IV. Sensor Design

The main sensor hardware consists of a brass open-ended pipe, and a microphone attached to one side of the pipe to form the closed end. The microphone collects the sound pressure at the closed end filtered by the acoustic cavity (i.e., the closed-open pipe). The pipe's fundamental resonant frequency is found by looking for the first maxima in the frequency spectrum. To avoid being confounded by features in the raw (unfiltered) ambient audio itself (including loud ambient sounds), a reference microphone is used to collect

 ISBN: 978-1-61208-297-4

environmental sounds not filtered by the pipe; this background spectrum is subtracted from the actual pretouch sensor channel. This noise cancellation approach substantially improves sensing accuracy. Figure 4 shows the system architecture of our seashell effect pretouch sensor.

A. Acoustic Design

Equations (2), (3), and (4) were employed throughout the acoustic design process. Although the end correction term is based on approximattion and not an exact solution, they serve as useful guiding references. The sensor acoustic characteristics are mainly determined by two geometric parameters: the pipe length L and the pipe radius a. Some considerarions should be taken when designing the two parameters:

(a) As a rule of thumb, we want the plane wave assumption to hold in order to have predictable acoustic behavior. It requires the resonance frequencies in the working range of the sensor to be lower than the first cut-off frequency in the circular pipe (ka<1.8412), so that only the fundamental mode will propagate.

(b) From (2), the end correction caused by the object (ΔL_{obj}) is roughly inversely proportional to the ratio h/a. It means using a larger pipe radius a could increase the amount of end correction changes at different object distances, and thus obtain better frequency resolution in the vertical sensing direction given a fixed pipe length L. Figure 2 shows the end correction values and the estimated resonance frequencies based on (2) and (4). From Fig. 2(a), we can see the frequency drops more at the close range when using larger radius (a=5 mm) compared to when using a small pipe (a=1 mm). This is due to the larger changes of the varying end correction term ΔL_{obj} caused by the object when using a larger radius. However, using a larger radius means the sensor will lose lateral sensing resolution physically, and become harder to integrating into the robot's gripper. Therefore, there is a trade-off when selecting the pipe radius.

(c) In the case of a fixed pipe radius a (fixed end correction ΔL and ΔL_{obj}), using a shorter pipe length L can result in more frequency shift according to (4). Figure 3 shows the shortest pipe (L=2.5mm) has the best dynamic range of the resonance frequency shift. The end correction changes is fixed because it is independent of L. Therefore, the shorter the pipe length L is, the more frequency shifts at the close distances. However, an open cavity is considered as a lumped-element (a mass) as a whole when the length is short compared to the wavelength ($kL_{eff} << 1$) [15], which has a different resonance behavior.

According to the above design considerations and experiments, a pipe length L=5 mm and radius a=2.5 mm was selected for our system, which has a compact size to be embedded on the PR2 gripper fingertip.

B. Hardware Design

A customized Printed Circuit Board (PCB) and fingertip structure was designed to hold all the electronic and mechanical components, including the microphone and the pipe. The cavity used in our system is a 2.5 mm radius / 5 mm length cylindrical pipe attached to a 2.5 mm radius / 3 mm length

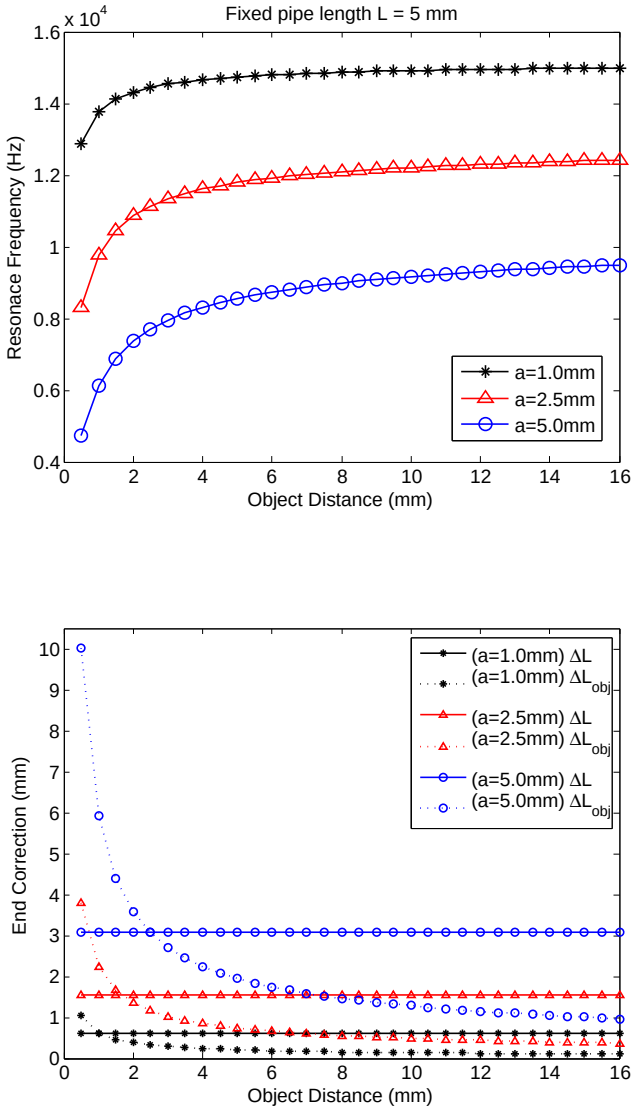

Fig. 2. (Upper:) resonance frequencies of the pipe at different distances with fixed length (L=5 mm) and various radius size. (Lower:) end correction of the pipe at different distances with fixed length and various radius size.

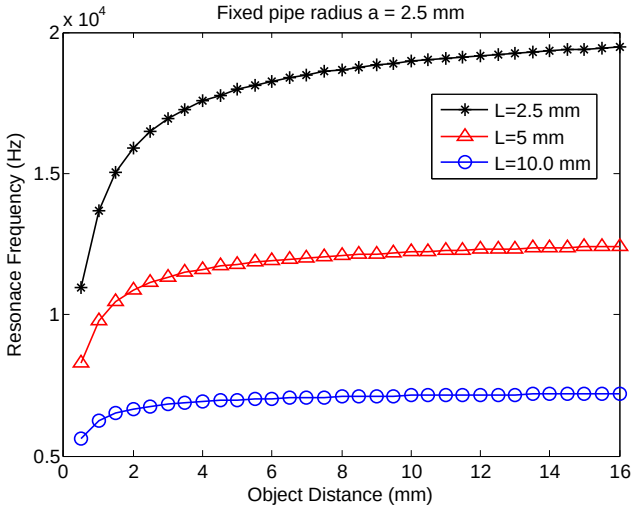

Fig. 3. The computed resonance frequencies of the pipe at different distances with fixed radius size (a=2.5mm) and various pipe length L.

 ISBN: 978-1-61208-297-4

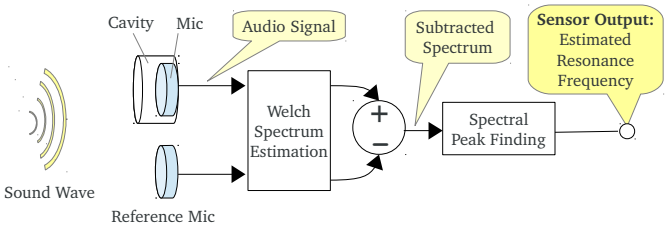

Fig. 4. The system architecture and the signal flow of the seashell effect pretouch sensor system.

microphone, which is compact enough to be embedded in the PR2 gripper's fingertip. Figure 1(b) shows the PCB and fingertip fixture with all the components attached, and Fig. 1(a) shows the completed pretouch sensing fingertip installed on the Willow Garage PR2's gripper. In the current implementation, there are two fingers on one of the grippers as the actual sensing channels, and a reference channel. The microphone for the sensing channel is attached with an acoustic cavity to amplify (attenuate) the ambient sound. The microphone for the reference channel is used to collect the ambient sound for spectrum subtraction. The only difference between the design is that the microphone on the reference channel is not attched to the pipe (acoustic cavity), so it simply collects the ambient (unfiltered) sound. Unlike the previous sensor [5], the new sensor described in this paper is completely integrated into the Willow Garage PR2 robot; all external cables and electronics have been eliminated. The embedded sensor design eliminates the constraints on robot arm motion caused by the external wires and electronics, and thus broadens the applicability of the sensors. The design presented here could also be adpated to integrate the sensor into other platforms.

The sound signal path implementation is decribed here. The pipe cavity filters the ambient noise, and the sound signal collected by an electret microphone (Panasonic WM61-A) is amplified by 40 dB through a low-noise microphone amplifier (Maxim MAX9814), and is sampled by the 8-bit Analog-To-Digital Convertor (ADC) on a 8-bit microcontroller (Atmel ATMega168). The sampled data is then transmitted from the microcontroller to the 8-bit soft soft processor (Xilinx PicoBlaze) residing in the FPGA inside the PR2's gripper via the Serial Peripheral Interface (SPI) communication protocol. Finally the sampled sound data is accessible from the FPGA to Robot Operating System (ROS) in the PR2 robot through the EtherCAT interface. The sampling rate for this whole signal path is 35,700 Hz for each channel. Currently, the sampling rate is limited by the SPI implementation on our circuit board; with more careful SPI design, the sampling rate could be increased up to the limit imposed by the microcontroller's ADC.

C. Signal Processing

The power spectral density of the sound signal from both channels are estimated using Welch spectrum estimation (N_s = 1024; overlap ratio = 70%; Hanning data taper). The spectrum of the reference channel is subtracted from the spectrum of the sensor signal before peak finding, which avoids the effect of loud sounds, outside of the sensor's frequency range, misleading the peak tracking. The peak finding and estimation

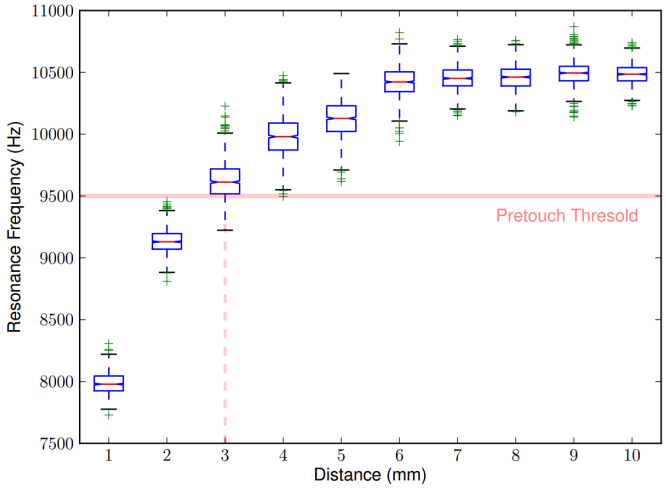

Fig. 5. The box-and-whisker plot of 1000 estimated resonance frequencies at each distance. It represents the sensor characteristics of the sensor with length L=5 mm and radius a=2.5 mm integrated on the robot fingertip.

algorithm we used here is the same as described in [5].

V. Characterization

In this section, we perform a set of experiments to characterize the sensor, including the resonance frequency shift at different object distance and effects of the object materials and ambient noise (the power density and spectral content).

A. Resonance Frequency Shift

The resonance frequency changes with object distance is evaluated by collecting 1000 sensor readings (filtered spectral peak frequency) at various distance from 1 mm to 10 mm. A box-and-whisker plot presents the performance of the sensor (Fig. 5). The resonance frequency drops at close distance starting from 6 mm. Based on experimental data, we select the a threshold at 9500 Hz (the lower quartile at 3 mm), such that the upper quartile at 3 mm is smaller than the lower quartile at 6 mm, so the sensor can be used as a binary sensor.

B. Material Sensitivity

The seashell effect pretouch sensor does not depend on optical or electrical material properties. Instead, it depends on mechanical / acoustic properties. This characteristic makes it a good complement to long range optical depth sensors. For example, seashell effect pretouch can sense highly transparent, reflective, or light-absorbing materials, which are difficult for optical sensors. In this section, we compare the sensor output for several different materials at the same distance. 1000 readings are measured for each object at a distance of 2 mm from the object's surface. The collected data is plotted in Fig. 6. The results show that the readings from materials with more porosity, such as cloth and foam, are more noisy than others. We hypothesize that these materials may acts as absorption or transparent materials depending on their thickness.

C. Effect of Ambient Sound

It is natural to wonder whether seashell effect pretouch could be improved by actively generating sound. Although

 ISBN: 978-1-61208-297-4

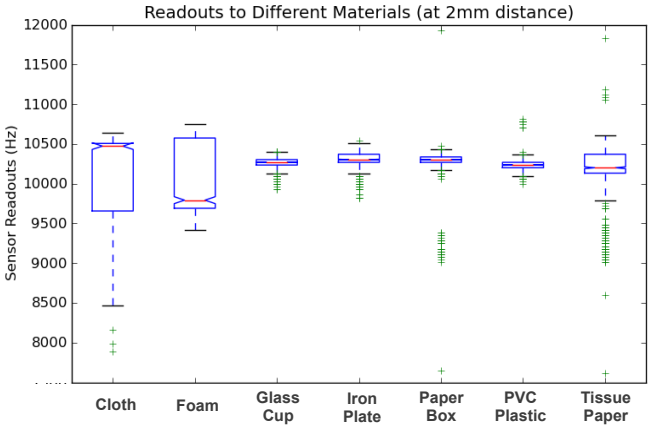

Fig. 6. The box plot of the sensor readouts to different materials. 1000 readouts are measured for each object at 2mm distance.

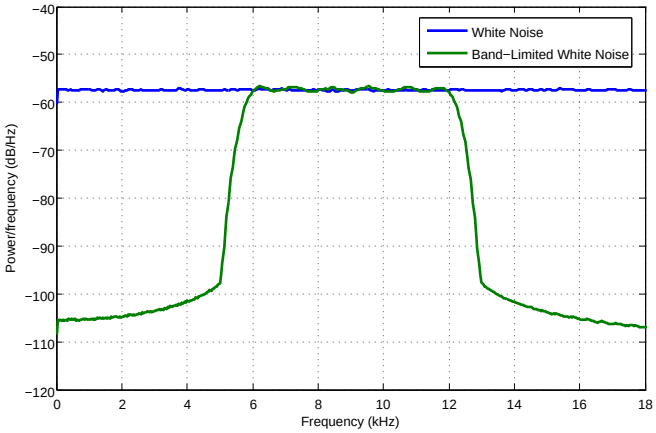

Fig. 7. The spectrum of the two waveforms used for external sound characterization. The bandlimited white noise is the white noise processed by a bandpass filter that attenuates below 6000 Hz and above 12000 Hz.

the passive scheme has the advantage of easy integration, it is desirable to understand how much improvement could be achieved if extra sound is actively generated. In this section, we systematically investigate the effects of deliberately generated sound; we will examine sensor performance as a function of the sound's spectral contents and power density. Finally, we describe an adaptive active sound generation scheme that maintains consistent sensor performace regardless of ambient sound conditions.

The first factor we investigate is the spectral contents of the sound. Two waveforms with different spectral contents are experimented and compared. The first waveform, white noise, has an uniform power spectral density distribution over its frequency band from 0 to 22,050 Hz. Considering the fact that the sensor's resonance frequency is always within a certain range, it is intuitive to hypothesize that providing bandlimited white noise might be sufficient, or even more efficient. Therefore, the second waveform has the uniform spectral density limited within 6,000 - 12,000 Hz (the relevant range, as determined in our previous experiments). The lower and upper bounds were determined by experimental data: the sensor readout is confined to this frequency band for objects in its working range (0 - 10 mm). The waveform is generated by processing the white noise waveform with a bandpass filter. Figure 7 shows the spectral density of the two different waveforms used in this experiment. (For example, 1.5 dB/Hz)

The second factor investigated is the power level of the added sound. During the experiment, we measure the average power density of the sound for 30 seconds without a stimulus, and again for 30s with the stimulus. (The average is computed first over time, and then over all discrete frequency bins.) The difference is computed to find the power increase due to the stimulus. The difference value in units of dB/Hz is the average power density level increased due to the generated sound stimulus. When the waveform is played, the amplitude is adjusted such that the total power received by the microphone is at the target level. Three sound levels are tested: without external stimulus sound, 0.5 dB/Hz stimulus, and 1.5 dB/Hz stimulus. The microphone selected for the sensor system has flat frequency response from a very low frequency (20 Hz) to its highest frequency (20,000 Hz), and the microphone amplifier has flat frequency response over 400 - 20,000 Hz according to the manufacturer's datasheet. Our seashell effect pretouch sensor works in the range of 6,000 - 12,000 Hz, so the effects of the system response of the microphone and amplifier can be considered uniform for both waveforms in this experiment.

Two indicators are defined to characterize the sensor performance: The CNR is defined as:

$$CNR := \frac{\overline{f_n} - \overline{f_1}}{\overline{\sigma(f_i)}}, i = 1..n \quad (5)$$

where i is the object distance in millimeter, n is the farthest distance, f are the measured resonance frequencies, and σ is the standard deviation. This is the frequency difference between the farthest (10mm) and closest (1mm) distance devided by the average of the standard deviation at each distance. It measures the ability of the sensor to distinguish between the farthest and closest distance, subject to sensor variability The second indicator Signal-To-Noise Ratio (SNR) is a measurement of how prominently the peak frequency stands out in the subtracted power spectral density compared with the noise level of the environment. It is defined as:

$$SNR := p_{max} - \overline{p} \quad (6)$$

where p is the power density (dB/Hz) of the spectrum. The higher the SNR is, the more likely the peak (resonance) frequency can be detected precisely in the spectrum. The first measure is useful for characterizing ground truth performance of the sensor. The second measure will be used autonomously to choose the energy of the stimulus. It is necessary for its autonomous use that this measure does not require knowledge of the ground truth.

Using the combination of two different waveforms and three different sound levels, five experimental trials were performed: no stimulus, 0.5 dB/Hz broadband stimulus, 0.5 dB/Hz bandimited stimulus, 1.5 dB/Hz broadband stimulus, and 1.5 dB/Hz bandimited stimulus. For each trial, 1000 readouts were measured at each distance from 1 to 10 mm (in increments of 1 mm). Figure 8 shows the power spectral densities and the computed SNR for the five trials. Whithout providing extra sound stimulus, the peak power is weak compared with the

 ISBN: 978-1-61208-297-4

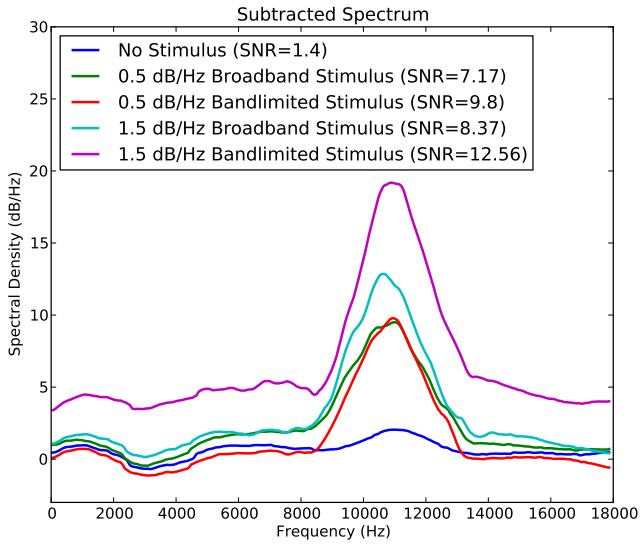

Fig. 8. The subtracted spectrum (spectrum of sensing channel - spectrum of reference channel) at 10mm distance when extra noise is played with different waveforms and different power.

environment sound, so any other noise bursting in the ambient sound can mislead the peak frequency estimation. By providing extra sound, the peak power at around 10,700 Hz is more prominent, so any other smaller peak appearing in the spectrum will not affect the peak frequency estimate. For the same stimulus power constraint, all the power in the bandlmited white noise stimulus falls in the sensor's working range (6,000 - 12,000 Hz), while the broadband stimulus essentially wastes some power (that outside the sensor's working region). Thus for the same allowed stimulus power, the bandlimited stimulus increases the sensor SNR more. Thus, the bandlimited white noise is more efficient, since we want to provide the smallest noise possible, both to avoid annoying nearby people who might hear the stimulus, and to prevent the robot / sensor system from expending unncessary electrical power.

The sensor readouts at each distance from 0 to 10 mm for each of the five cases; the CNR is computed for each case. From Fig. 9, it is clear to see without providing external stimulus noise in a quiet environment, the sensor readings are spread out, with no prominent peaks. When bandlimited white noise is provided at the average power density of 1.5 dB/Hz, the CNR is improved from 0.9 to 10.88 compared to the case without extra noise. (Note that in our prior work [5], noise sources in the robot such as fans appear enabled better performance than the no stimulus case presented here; this data was taken in a quiet room far from the robot.)

Table I shows the performance indices for all the experiment sets. From these results, we can conclude the following: (1) appropriate ambient noise spectrum and level is essential for good sensor performance. (2) the bandlimited white noise is more efficient to imporve the SNR and CNR compared with the white noise at the same power level. (3) CNR is hightly correlated with SNR, which matches the intuition that the more prominent peak will facilitate the peak estimation, and thus the sensor measurement is more accurate. Based on these findings, we propose to implment an adaptive stimulus noise generation

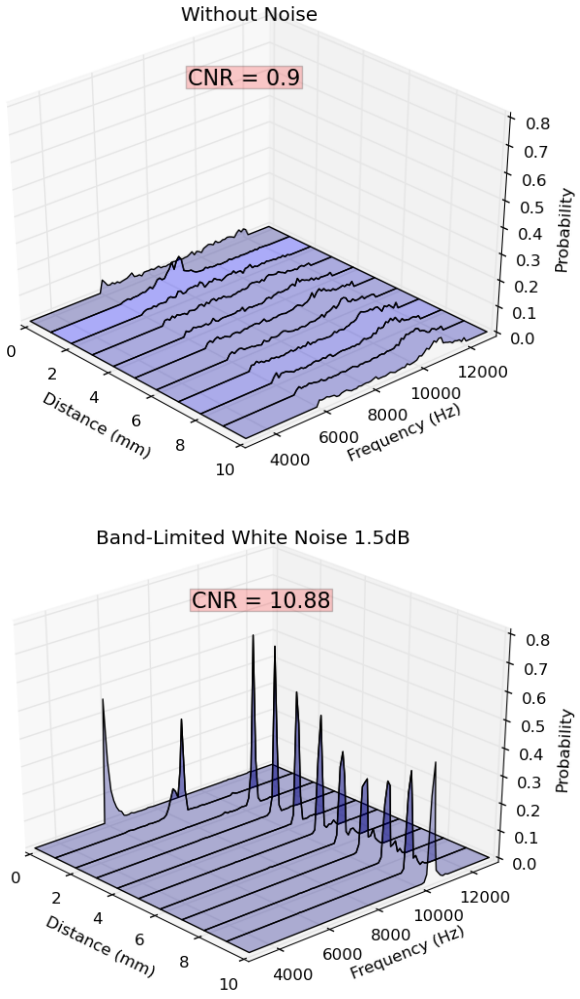

Fig. 9. The sensor model created by collecting 1000 sensor readouts at each distance from 0 to 10 mm for the two cases: (a) In a quiet room without actively providing extra noise. (b) the extra bandlimited white noise provided at 1.5 dB/Hz average spectral power density.

TABLE I. EFFECT OF THE EXTRA NOISE SPECTRUM ON SENSOR PERFORMANCE

Waveform	Stimulus Noise Average Power Density (dB/Hz)	CNR	SNR
No Extra Noise	0	0.90	1.40
White Noise	0.5	6.57	7.17
Bandlimited White Noise	0.5	9,37	9.80
White Noise	1.5	8.45	8.37
Bandlimited White Noise	1.5	10.88	12.56

scheme described in the following section.

D. Adaptive Stimulus Generation

The goal of the adaptive stimulus sound generation scheme is to maintain a consistent and quantifiable sensor performace regardless of ambient noise conditions. Based on the findings from the experiments, bandlimited white noise is selected as the sound waveform of the stimulus sound. We can hypothisize that if the SNR in the sound signal spectrum is kept at a fixed value, the actual sensor measurement performance indicator SNR will also be maintained at a stable level. Since

 ISBN: 978-1-61208-297-4

CNR can only be computed with knowledge of the ground truth sensing situation, it is not the appropriate quantity to control the adaptive stimulus generation. In this particular implementation, a SNR target of 10 was selected, as suggested by the experimental data. A first order closed-loop feedback control is used to monitor the current SNR in the spectrum from the sensor and adjust the bandlimited white noise level with a fixde gain. The goal is to keep the SNR to the targeted value, so that consistent sensor performace can be achieved.

To assess the effectiveness of this approach, the standard deviation of the sensor readouts is computed from the readouts in 60 seconds for both the cases with and without the adaptive stimulus noise generation while the robot's ego noise presents. The standard deviation decreases from 183.59 to 53.56 Hz when the adaptive stimulus is applied. (The discrete frequency bin size is 69.72 Hz). A demonstration of the effectiveness of this scheme can be seen in the video attachment (address in the next section), in which the realtime sensor readouts and the change of stimulus volume are visualized.

VI. APPLICATION IN ROBOTICS: OBJECT CONTOUR TRACKING

The embedded sensor design eliminates the robot arm's motion constraints caused by the external cables and electronics, and thus broadens the sensor's applicability. It also makes it feasible to put one sensor in each of the PR2 robot's fingers. This enables differential distance measurements, and thus allows the robot to orientate its fingertup towards the surface of the object. Using this capability, we present an object contour tracking as an application example to demonstrate the capabilities of the sensor. Two sensors are installed on the same robotic gripper, and the difference between the two sensor readings are used to compute the orientation of the fingertip with respect to the object. Three objects with different material properties are tested: mug (non-conductive material), glass cup (transparent material), and a stainless pot (highly reflective material). The objects are those the previous electric-field and optical pretouch sensors have trouble to sense. These examples demonstrate the PR2 collecting local geometric information enabled by the pretouch sensors, and allows the robot gripper to successfully follow the contour of the objects even if they are transparent or highly reflective.

VII. CONCLUSIONS AND FUTURE WORK

A. Conclusions

This paper demonstrated a novel acoustic pretouch sensor inspired by the well-known seashell effect. As far as we know, this effect has not previously been used to build proximity sensors. We characterize the frequency shift of the sensor at different object distance, and the effect of ambient noise on the sensor performance, including the noise level and spectral content. A stimulus consisting of band-limited white noise with frequency content in the sensor's working frequency range is most effective, compared with a broadband stimulus, or random ambient sound. An automatic adaptive stimulus noise compensation scheme, which detects the current ambient sound condition and provides additional band-limited whitnoise, was proposed to maintain a consistent SNR in the spectrum, and thus achieve the good performance of the sensor invariant to the ambient sound.

The fully-integrated sensor into the robot grippers makes it feasible to put one sensor in each of the PR2 robots fingers for differential distance measurement, and thus enables the object contour tracking application. Compared to to conventional sonar based on time of flight measurements, the technique we presented based on incoherent peak following has a number of practical benefits: (1) The sound stimulus source can be located anywhere—it does not have to be close to the sound receiver, which is an advantage for sensor integration into devices; (2) careful/short-interval time measurements are not required, and (3) our scheme should not be affected by multi-path effects commonly seen when using time of flight sonar methods.

B. Future Work

More applications using the proposed sensor systems are working in progress. For example, the sensor can be integrated with the existing microphones in a mobile phone as a proximity sensor to trigger the lock of the touch screen when the objects (human ears) are close to the microphone to prevent touching the screen by mistake while speaking (current mobile phones use an dedicated light sensor for that purpose).

REFERENCES

[1] J. R. Smith, E. Garcia, R. Wistort, and G. Krishnamoorthy, "Electric field imaging pretouch for robotic graspers," in IEEE/RSJ International Conference on Intelligent Robots and Systems, 2007, pp. 676–683.

[2] R. Wistort and J. R. Smith, "Electric field servoing for robotic manipulation," in IEEE/RSJ International Conference on Intelligent Robots and Systems, 2008, pp. 494–499.

[3] B. Mayton, L. LeGrand, and J. R. Smith, "An electric field pretouch system for grasping and co-manipulation," in IEEE International Conference on Robotics and Automation, 2010, pp. 831–838.

[4] K. Hsiao, P. Nangeroni, M. Huber, A. Saxena, and A. Y. Ng, "Reactive grasping using optical proximity sensors," in IEEE International Conference on Robotics and Automation, 2009, pp. 2098–2105.

[5] L.-T. Jiang and J. R. Smith, "Seashell effect pretouch sensing for robotic grasping," in IEEE International Conference on Robotics and Automation, 2012, pp. 2851–2858.

[6] L.-T. Jiang and J. R. Smith, "A unified framework for grasping and shape acquisition via pretouch sensing," in IEEE International Conference on Robotics and Automation, 2013.

[7] L. Arapan, E. Anderas, I. Katardjiev, and V. Yantchev, "Sensitivity features of thin film plate acoustic wave resonators," IEEE Sensors Journal, 2011, vol. 11, no. 12, pp. 3330–3331.

[8] H. Zhang and E. Kim, "Micromachined acoustic resonant mass sensor," Journal of Microelectromechanical Systems, 2005, vol. 14, no. 4, pp. 699–706.

[9] H. Zhang, M. Marma, S.Bahl, E. Kim, and C. McKenna, "Sequence specic label-free dna sensing using film-bulk-acoustic-resonators," IEEE Sensors Journal, 2007, vol. 7, no. 12, pp. 1587–1588.

[10] J. W. Coltman, "Differentiating sonar reflections from corners and planes by employing an intelligent sensor," Journal of the Acoustical Society of America, 1978, vol. 65, pp. 499–506.

[11] L. V. King, "On the electrical and acoustic conductivities of cylindrical tubes bounded by infinite flanges," Journal of the Acoustical Society of America, 1936, vol. 21, pp. 128–144.

[12] H. Levine and J. Schwinger, "On the radiation of sound from an unflanged circular pipe," Physical Review, 1948, vol. 73, pp. 383–406.

[13] A. R. D. Silva, P. H. Mareze, and A. Lenzi, "Approximate expressions for the reflection coefficient of ducts terminated by circular flanges," Journal of Brazil Society of Mechenical Science and Engineering, 2012, vol. 34, no. 2, pp. 219–224.

[14] J.-P. Dalmont, C. Nederveen, and N. Joly, "Radiation impedance of tubes with different flanges: Numerical and experimental investigations," Journal of Sound and Vibration, 2001, vol. 244, no. 3, pp. 505–534.

[15] D. T. Blackstock, Fundamentals of Physical Acoustics, 1st ed., Wiley-Interscience, 2000.

 ISBN: 978-1-61208-297-4